Image Series Expansion for Electrical Impedance Tomography

M. Dolgin and P. D. Einziger

Department of Electrical Engineering, Technion-Israel Institute of Technology, Haifa, Israel

(Received 5 May 2004; published 28 September 2004)

A novel electrical impedance tomography method is introduced for reconstruction of layered biological tissues. The method utilizes a recently proposed image series expansion scheme in conjunction with the WKB approximation. This results in a locality feature, assigning analytically to each image term a local impedance associated with a unique layer, and thus leading to linear, efficient, and accurate reconstruction procedures.

DOI: 10.1103/PhysRevLett.93.148101 PACS numbers: 87.63.Pn, 02.30.Zz, 03.50.De, 41.20.Cv

The estimation of electrical parameters associated with biological tissues via electrical impedance tomography (EIT) has recently become of increased scientific and public interest [1–3]. Here, we focus on a novel EIT method utilizing a recently proposed quasistatic image series expansion scheme for layered media [4] in conjunction with the WKB approximation [5]. The resultant WKB image series expansion is characterized by an outstanding feature, namely, each image term corresponds analytically and explicitly to a unique layer, leading to a one to one mapping between each image term and the local impedance of the associated layer. This locality feature leads to an effective linear reconstruction of the electrical impedance profile via Legendre expansion in conjunction with Prony's method (PM) and image peeling (IP). Computations based on our novel procedures, including noisy data, provide accurate, efficient, and stable reconstruction, particularly when relatively small datebase and, consequently, shallow penetration are required.

Quasistatic fields representation in plane-stratified media, a well-known and an intensively discussed topic (e.g., [4,6]), is briefly reviewed here for the sake of clarity and completeness. The physical configuration of our problem, depicted in Fig. 1, consists of a time-harmonic current point source S, an observation point P, and $n+1$ homogeneous layers. The parameter $\sigma(z)$ denotes the piecewise constant conductivity of the medium, i.e., $\sigma(z)=\sigma_i$, in the ith layer, $z_{i-1}<z<z_i$, $i=1,2,\ldots,n+1$, $z_0=-\infty$, $z_{n+1}=\infty$. We note that $\sigma(z)$ should be replaced by the complex conductivity $\varsigma(z)=\sigma(z)+j\omega\varepsilon(z)$, in every layer, for which the inequality $\sigma(z)\gg j\omega\varepsilon(z)$ is not satisfied. The parameters $\varepsilon(z)$ and ω denote the medium permittivity and the angular (low) frequency of the electrode excitation (assuming time dependence $e^{j\omega t}$), respectively. The quasistatic electromagnetic field can be expressed via a potential distribution, which has been expended recently into the following rigorous image series representation [4],

$$\Phi(\mathbf{r},\mathbf{r}')=\frac{I}{4\pi\sigma_1}\left[\frac{1}{|\mathbf{r}-\mathbf{r}'|}+\sum_{l_1=0}^{1}\sum_{m_1=0}^{\infty}\cdots\sum_{l_{n-1}=0}^{s_{n-2}}\sum_{m_{n-1}=0}^{\infty}\left\{\prod_{k=1}^{n-1}\binom{s_{k-1}+1}{l_k}\binom{s_k}{m_k}K_k^{l_k}[1-K_k^2]^{s_{k-1}-l_k+1}[-K_k]^{m_k}K_n^{m_k-l_k}\right\}\frac{K_n}{|\mathbf{r}-\tilde{\mathbf{r}}_k'|}\right], \tag{1}$$

where $\mathbf{r}$ and $\tilde{\mathbf{r}}_k'$, denoting the observation and the image points, are given via

$$\mathbf{r}=(x,y,z)\quad\text{and}\quad\tilde{\mathbf{r}}_k'=(0,0,\tilde{z}_k'), \tag{2}$$

respectively, and

$$\tilde{z}_k'=2\sum_{k=1}^{n-1}(s_k+1)(z_{k+1}-z_k)-z', \tag{3}$$

$$s_n=\sum_{k=1}^{n}(m_k-l_k),\qquad s_0=0. \tag{4}$$

In the WKB limit [5], the intrinsic reflection coefficients K_i, $i=2,3,\ldots,n$, given by

$$K_i=\frac{\sigma_i-\sigma_{i+1}}{\sigma_i+\sigma_{i+1}},\qquad K_0=0,\qquad \sigma_0=\sigma_1, \tag{5}$$

are assumed to be sufficiently small, i.e.,

$$|K_i|\ll 1. \tag{6}$$

Hence, maintaining image terms of $O(|K_i|)$, the expression in (1) is readily reduced into the WKB image series expansion,

$$\Phi_{\mathrm{WKB}}(\mathbf{r},\mathbf{r}')=\frac{I}{4\pi\sigma_1}\left[\frac{1}{|\mathbf{r}-\mathbf{r}'|}+\frac{K_1}{|\mathbf{r}-\mathbf{r}_1'|}+(1-K_1^2)\sum_{i=2}^{n}\frac{K_i}{|\mathbf{r}-\mathbf{r}_i'|}\right],$$
$$\mathbf{r}_i'=(0,0,-2z_i-z'). \tag{7}$$

Note that the intrinsic reflection coefficient K_1^2 is contained, however, in (7) to accommodate the case $\sigma_1=0$, leading to a non-WKB coefficient $K_1=-1$.

The basic "backscattering" reconstruction setup is depicted in Fig. 1, setting $\sigma_1=0$. Both the excitation current source I and the measured potential $V(\rho)$ are confined to the plane $z=z'=0$, where $\rho=\sqrt{x^2+y^2}$ denotes the radial distance. The potential $V(\rho)$ can be

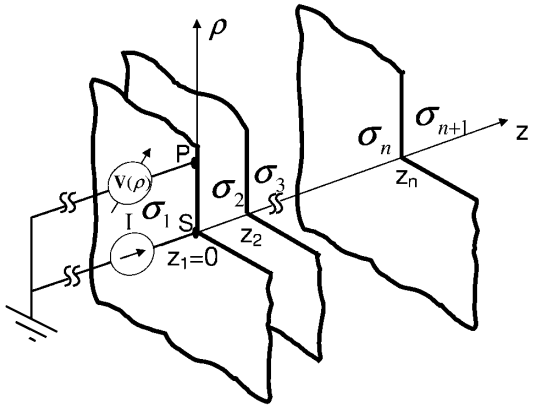

FIG. 1. Physical configuration and reconstruction setup.

expressed, via (7), as

$$V(\rho) = \Phi_{\mathrm{WKB}}(\mathbf{r}, \mathbf{r}')|_{z=z'=0,\sigma_1=0} = \frac{I}{\pi\sigma_2}\left[\frac{1}{2\rho} + \sum_{i=2}^{n} \frac{K_i}{[\rho^2 + (2z_i)^2]^{1/2}}\right]. \quad (8)$$

Evidently, Eq. (8) contains all the information required for reconstruction of the layered media. Evaluation of an individual ith image term in (8) leads to reconstruction of K_i and z_i and, consequently, the electrical impedance $\sigma(z)$ of the entire medium [via Eq. (5)]. While the standard least squares (LS) nonlinear optimization procedure seems capable of obtaining the desired information regarding the unknown image terms, its execution for a large number of images usually results in cumbersome global minimum estimation and, thus, unacceptable computation time, as expected for a nonlinear algorithm. Herein, we seek an alternative linear procedure, which has the potential of accurately reconstructing a relatively large number of layers (i.e., distinct image terms) and significantly reducing the execution time (relative to the LS procedure).

Noting that the geometrical parameters z_i are associated with the singularities of $V(\rho)$ in the complex ρ plane, whereas the electrical parameters K_i are associated with their weights, one is tempted to perform the reconstruction procedure via analytic continuation of $V(\rho)$ into the complex domain. Such an approach is always possible for an analytic operator (Laplace's equation) relying on analytic data [7]. However, in view of the well-known unstable properties of analytic continuation procedures, we focus here on real function analysis, namely, determination of the radius of convergence of each image in the real ρ axis rather than detecting its singularity in the complex ρ plane. To this end, standard Taylor series expansion of $V(\rho)$ in (8) is equivalently expressed via orthogonal Legendre polynomial expansion, thereby effectively evaluating the expansion coefficients by inner products. Since $0 \le \rho < \infty$, we use shifted Legendre polynomial [8] $L_l(1 - 2\rho^2)$, defined on a unit window width $0 \le \rho \le w$, $w = 1$, to expand the scaled potential $V(s\rho)$ (with respect to the Legendre's unit window width $0 \le \rho \le 1$), leading to

$$V(s\rho) = \sum_{l=0}^{\infty} b_l(s) L_l(1 - 2\rho^2), \quad (9)$$

where [9]

$$b_l(s) = 2(2l+1)\int_0^1 \rho V(s\rho) L_n(1-2\rho^2)\,d\rho = \frac{2(2l+1)}{s^2}\int_0^s \rho V(\rho) L_n[1-2(\rho/s)^2]\,d\rho = \frac{2I}{\pi s\sigma_2}\sum_{i=1}^{n} \mathcal{K}_i[2z_i/s + \sqrt{1+(2z_i/s)^2}]^{-(2l+1)}, \quad (10)$$

and s is a positive real scaling factor. Note that s can also be regarded, via the second equality in Eq. (10), as a scaling factor for Legendre's unit window width $w = 1$ [with respect to a nonscaled potential $V(\rho)$]. Furthermore, while for $i > 1$, $\mathcal{K}_i = K_i$, for $i = 1$, $\mathcal{K}_1 = 1/2$, and the unknown parameter is σ_2.

It is readily recognized that the individual n terms contained in the right-hand side summation of Eq. (10) may be regarded as n distinct exponentials $[2z_i/s + \sqrt{1 + (2z_i/s)^2}]^{-2}$ of power l, weighted by $2I\mathcal{K}_i[2z_i/s + \sqrt{1 + (2z_i/s)^2}]^{-1}/(\pi s\sigma_2)$. Hence, the PM procedure [10] exploiting $2n$ data points, i.e., $b_l(s)$, $0 \le l \le 2n-1$ or, equivalently, $2n$ inner products, can be utilized to reconstruct n distinct exponentials and weights characterizing the stratification geometry and electrical parameters, respectively. Also, to avoid dominance of any one of the exponentials contained in the right-hand side of Eq. (10) the scaling factor s should be large enough to support the entire reconstruction range, i.e.,

$$s \ge 2z_i/w, \quad (11)$$

leading to the inclusion of $V(\rho)$ well within the window $0 \le \rho/w \le s$. Note, however, that the selection $s \gg 2z_n/w$ results in almost linearly dependent exponentials and, thus, should be avoided.

Following the PM procedure, the n unknown exponentials $[2z_i/s + \sqrt{1 + (2z_i/s)^2}]^{-2}$ are roots of the n order polynomial equation

$$\sum_{p=0}^{n} c_p(\mu^2)^p = 0, \quad (12)$$

where $c_n = 1$. Let μ_i^2 denote the ith root of (12), then,

$$\mu_i = [2z_i/s + \sqrt{1 + (2z_i/s)^2}]^{-1}, \quad (13)$$

leading to

$$z_i = \frac{\mu_i^2 - 1}{4\mu_i} s. \quad (14)$$

The polynomial coefficients denoted by the vector $\mathbf{C} = [c_0, c_1, \ldots, c_{n-1}]^T$ are solutions of the linear system,

TABLE I. WKB reconstruction via the PM procedure for (a) oscillating and (b) positive intrinsic reflection coefficients $\mathcal{K}_i$ ($w = 1$, $s = 2$, $\sigma_{2,\text{exact}} = 10S/m$). Results for noisy data ($\text{SNR}|_{\rho=s_5 w} = 60$ dB, $s_5 = 15$) are contained in square brackets.

	Layer i	z_i/w exact	z_i/w reconstructed	Error (%)	$\mathcal{K}_i$ exact	$\mathcal{K}_i$ reconstructed	Error (%)	$\frac{\sigma_{i+1,\text{exact}}}{\sigma_{2,\text{exact}}}$	$\frac{\sigma_{i+1,\text{reconst}}}{\sigma_{2,\text{exact}}}$	Error (%)
(a)	1	0	-1×10^{-6} [-7×10^{-6}]	0 [0]	0.5	0.5 [0.5]	0 [0]	1.0	1.0 [1.001]	0.007 [0.05]
	2	0.1	0.0997 [0.097]	0.25 [3.05]	0.1	0.0994 [0.092]	0.58 [8.27]	0.818	0.819 [0.832]	0.12 [1.73]
	3	0.2	0.201 [0.216]	0.43 [8.16]	−0.1	−0.099 [−0.100]	0.95 [0.09]	1	0.999 [1.017]	0.07 [1.75]
	4	0.5	0.502 [0.473]	0.43 [5.48]	0.09	0.090 [0.096]	0.35 [6.47]	0.835	0.835 [0.840]	0.005 [0.6]
	5	2	2.009 [2.064]	0.43 [3.21]	−0.15	−0.150 [−0.149]	0.33 [0.59]	1.130	1.131 [1.134]	0.1 [0.38]
(b)	1	0	3×10^{-7} [-3×10^{-5}]	0 [0]	0.5	0.5 [0.5]	0 [0]	1.0	1.0 [1.0001]	0.0003 [0.01]
	2	0.1	0.0999 [0.101]	0.04 [0.85]	0.1	0.0999 [0.104]	0.14 [3.9]	0.818	0.818 [0.812]	0.029 [0.77]
	3	0.2	0.199 [0.208]	0.23 [4.21]	0.1	0.099 [0.100]	1.5 [0.26]	0.670	0.672 [0.664]	0.33 [0.83]
	4	0.5	0.499 [0.535]	0.22 [6.96]	0.09	0.086 [0.086]	4.6 [4.62]	0.559	0.565 [0.559]	1.17 [0.01]
	5	2	2.072 [2.224]	3.6 [11.2]	0.15	0.147 [0.135]	2.2 [9.99]	0.413	0.421 [0.426]	1.85 [3.11]

$$\mathbf{A}\,\mathbf{C} = \mathbf{B}, \qquad \mathbf{C} = \mathbf{A}^{-1}\mathbf{B}, \tag{15}$$

where $\mathbf{A}_{j,k} = b_{j+k-1}(s)$, $j,k = 0,1,\ldots,n-1$, $\mathbf{B} = -[b_n(s), b_{n+1}(s),\ldots,b_{2n-1}(s)]^T$, and T denotes the transpose operation. Finally, the weight coefficients, denoted by the vector $\mathbf{K} = 2I[\mu_1\mathcal{K}_1, \mu_2\mathcal{K}_2, \ldots, \mu_n\mathcal{K}_n]^T/(\pi s\sigma_2)$, are also solutions of the linear system

$$\mathbf{M}\,\mathbf{K} = \mathbf{D}, \mathbf{K} = \mathbf{M}^{-1}\mathbf{D}, \tag{16}$$

where $M_{i,j} = (\mu_j^2)^i$ and $\mathbf{D} = [b_0(s), b_1(s), \ldots, b_{n-1}(s)]^T$.

The potential promise of the outlined method [Eqs. (12)–(16)] is now demonstrated via numerical simulations. As already noted, the selection of the scaling factor s determines the maximal reconstruction depth. The number of Legendre coefficients b_l is finite and limited since high order coefficients, associated with high order inner products (numerical integrations) involving high order Legendre polynomials, are difficult to calculate due to a highly oscillating integrand. This, of course, establishes a bound on the maximal number of layers that can be reconstructed and seems to be an inherent limitation of a quasistatic-type reconstruction method. The results summarized in Table I reveal that a very good reconstruction can be obtained via the PM procedure for five layers of WKB medium, even for noisy data, i.e., SNR = 60 dB (e.g., [11]) at the end point of the widest Legendre window. The successful reconstruction demonstrated in Table I(a), for oscillating intrinsic reflection coefficients $\mathcal{K}_i$, is due to the excellent agreement between the WKB potential $V(\rho)$ in (8) and the exact potential $\Phi(\mathbf{r},\mathbf{r}')|_{z=z'=0,\sigma_1=0}$ in (1), as depicted in Fig. 2. This excellent agreement is due to the oscillating reflection coefficients, leading to fast convergence of the image series expansion in (1) and, thus, to minimization of the truncation error caused by non-WKB image terms that have been neglected in (8). This, however, is not the case for positive intrinsic reflection coefficients, as depicted in Fig. 2, leading to somewhat less accurate reconstruction results [Table I(b)].

The IP procedure is based on precise identification of the ith image term [Eq. (8)], located in the closest vicinity of the setup plane (associated with the closest layer), and subsequently of both z_i and K_i. Then, subtract its contribution to the potential $V(\rho)$ in (8) and repeat the process. This procedure is terminated then either once all the n images are identified and peeled out or when the numerical noise associated with the successive peelings (substractions) governs. Evidently, successful execution of the IP procedure can be carried out by appropriately adjusting the scaling factor s to enhance the image contribution corresponding to the smallest z_i, in (10). Consequently, the scaling factor s_p for each peeling step p of the algorithm has to satisfy the inequality

$$2z_p/w < s_p < 2z_{p+1}/w. \tag{17}$$

Note that, as p approaches n, the IP scaling factor in (17) approaches that of PM in (11). The resultant coefficient $b_l^p(s_p)$, expressed as

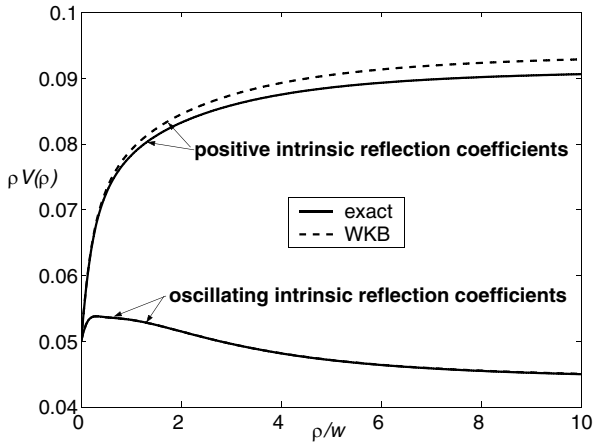

FIG. 2. Normalized WKB and exact potentials ($\rho V(\rho)$ and $\rho\Phi(\mathbf{r},\mathbf{r}')|_{z=z'=0,\sigma_1=0}$ in (8) and (1), respectively), versus normalized radial distance ρ/w ($w = 1$).

TABLE II. WKB reconstruction via the IP procedure for (a) oscillating and (b) positive intrinsic reflection coefficients $\mathcal{K}_i$ ($w = 1$, $\sigma_{2,\text{exact}} = 10S/m$). Results for noisy data (SNR $|_{\rho=s_5 w}$ = 60 dB, $s_5 = 15$) are contained in square brackets.

	Layer i	s_i	z_i/w exact	z_i/w reconstructed	Error (%)	$\mathcal{K}_i$ exact	$\mathcal{K}_i$ reconstructed	Error (%)	$\frac{\sigma_{i+1,\text{exact}}}{\sigma_{2,\text{exact}}}$	$\frac{\sigma_{i+1,\text{reconst}}}{\sigma_{2,\text{exact}}}$	Error (%)
(a)	1	0.01	0	0 [0]	0 [0]	0.5	0.5 [0.5]	0 [0]	1.0	1.0 [1.005]	0 [0.45]
	2	0.25	0.1	0.100 [0.1003]	0.002 [0.3]	0.1	0.0999 [0.0995]	0.04 [0.52]	0.818	0.818 [0.823]	0.01 [0.56]
	3	1	0.2	0.201 [0.206]	0.56 [2.92]	−0.1	−0.102 [−0.101]	1.56 [0.49]	1.0	1.003 [1.007]	0.32 [0.66]
	4	4	0.5	0.477 [0.483]	4.66 [3.40]	0.09	0.085 [0.081]	5.34 [10.3]	0.835	0.846 [0.856]	1.30 [2.55]
	5	15	2.0	2.126 [2.281]	6.30 [14.0]	−0.15	−0.146 [−0.148]	2.8 [1.12]	1.13	1.135 [1.154]	0.44 [2.20]
(b)	1	0.01	0	0 [0]	0 [0]	0.5	0.5 [0.5]	0 [0]	1.0	1.0 [1.0]	0 [0]
	2	0.25	0.1	0.099 [0.098]	0.01 [1.62]	0.1	0.0999 [0.092]	0.10 [7.58]	0.818	0.818 [0.831]	0.02 [1.54]
	3	1	0.2	0.199 [0.185]	0.38 [7.32]	0.1	0.098 [0.0998]	1.85 [0.16]	0.669	0.672 [0.68]	0.40 [1.58]
	4	4	0.5	0.501 [0.516]	0.20 [3.17]	0.09	0.088 [0.1058]	2.51 [17.55]	0.559	0.564 [0.55]	0.85 [1.61]
	5	15	2	2.165 [2.289]	8.25 [14.5]	0.15	0.156 [0.1239]	4.29 [17.37]	0.413	0.411 [0.429]	0.47 [3.75]

$$b_l^p(s_p) = \frac{2I\mathcal{K}_p}{\pi s_p \sigma_2 (2z_p/s_p + \sqrt{1+(2z_p/s_p)^2})^{2l+1}} \left[1 + \sum_{i=p+1}^{n} \frac{\mathcal{K}_i}{\mathcal{K}_p} \left(\frac{2z_p/s_p + \sqrt{1+(2z_p/s_p)^2}}{2z_i/s_p + \sqrt{1+(2z_i/s_p)^2}} \right)^{2l+1} \right] \sim \frac{2I\mathcal{K}_p}{\pi s_p \sigma_2 (2z_p/s_p + \sqrt{1+(2z_p/s_p)^2})^{2l+1}}, \quad (18)$$

indeed, equals asymptotically the pth image contribution, for sufficiently large l. Finally, taking the logarithm of (18) for large l, i.e.,

$$\ln b_l^p(s_p) \sim \ln\left(\frac{2I\mathcal{K}_p}{\pi s_p \sigma_2}\right) - (2l+1)\ln\left(\frac{2z_p}{s_p + \sqrt{1+(\frac{2z_p}{s_p})^2}}\right) = D_p + E_p l, \quad (19)$$

followed by the first order polynomial LS fit, results in explicit expressions for z_p and $\mathcal{K}_p$,

$$2z_p = s_p \sinh(E_p/2), \quad \mathcal{K}_p = \frac{\pi s_p \sigma_2}{2I} \exp(D_p + E_p/2), \quad (20)$$

respectively, where D_p and E_p are real constants defined in (19).

The IP procedure is demonstrated in Table II for the same parameters specified in Table I and Fig. 2. It is readily noted that while the IP procedure (Table II) leads to more accurate results than the PM procedure (Table I) for the first few layers, the results corresponding to the subsequent layers are inferior to those obtained via the PM procedure due to numerical noise accumulation, an inherent disadvantage of the IP method. This observation holds effectively for noisy data as well, i.e., for SNR = 60 dB (e.g., [11]) at the end point of the widest Legendre window. Evidently, the oscillating reflection coefficients lead to more accurate WKB approximation (Fig. 2), resulting in an effective IP reconstruction procedure for deeper layers.

The potential promise of the novel EIT reconstruction procedures presented herein has been demonstrated via numerical simulations, including noisy data. Two linear quasistatic reconstruction procedures have been introduced: the PM procedure and the IP procedure. Both methods are efficient for shallow reconstruction due to the following factors: (i) accuracy limitation in calculation of higher order Legendre coefficients (determining the maximal number of layers); (ii) constraints (11) and (17), for the PM and the IP algorithms, respectively [effective regularization conditions, stemming from the direct problem solution (8)] cannot be satisfied simultaneously for both shallow and deep layers (e.g., the fifth layer in Table I); (iii) numerical noise accumulation for the IP method. These procedures can be extended for non-WKB profiles provided that WKB image series expansion in (7) is replaced by its rigorous image series representation (1)–(5).

[1] B. H. Brown, J. Med. Eng. Technol. **27**, 97 (2003).
[2] *Electrical Impedance Tomography*, edited by J. G. Webster (IOP, Bristol, UK, 1990).
[3] J. G. Berryman and R. V. Kohn, Phys. Rev. Lett. **65**, 325 (1990).
[4] P. D. Einziger, L. M. Livshitz, and J. Mizrahi, IEEE Trans. Antennas Propagat. **50**, 1813 (2002).
[5] P. M. Morse and H. Feshbach, *Methods of Theoretical Physics* (McGraw-Hill, New York, 1953).
[6] J. R. Wait, *Geo-Electromagnetism* (Academic Press, New York, 1982).
[7] R. Courant and D. Hilbert, *Methods of Mathematical Physics* (Wiley, New York, 1989).
[8] M. Abramowitz and I. A. Stegun, *Handbook of Mathematical Functions* (Dover Publications, New York, 1970).
[9] A. Erdelyi, *Tables of Integral Transforms* (McGraw-Hill, New York, 1954), Vol. II.
[10] R. W. Hamming, *Numerical Methods for Scientists and Engineers* (Dover, New York, 1986).
[11] A. F. Frangi *et al.*, IEEE Trans. Med. Imag. **21**, 566 (2002).